CrossMark

RESEARCH PAPER

Investigation of Coulomb stress changes in south Tibet (central Himalayas) due to the 25th April 2015 M_W 7.8 Nepal earthquake using a Coulomb stress transfer model

Xu Cheng · Guojie Meng

Abstract After M_W 7.8 Nepal earthquake occurred, the rearrangement of stresses in the crust commonly leads to subsequent damaging earthquakes. We present the calculations of the coseismic stress changes that resulted from the 25th April event using models of regional faults designed according to south Tibet-Nepal structure, and show that some indicative significant stress increases. We calculate static stress changes caused by the displacement of a fault on which dislocations happen and an earthquake occurs. A M_W 7.3 earthquake broke on 12 May at a distance of ∼ 130 km SEE of the M_W 7.8 earthquake, whose focus roughly located on high Coulomb stress change (CSC) site. Aftershocks (first 15 days after the mainshock) are associated with stress increase zone caused by the main rupture. We set receiver faults with specified strikes, dips, and rakes, on which the stresses imparted by the source fault are resolved. Four group normal faults to the north of the Nepal earthquake seismogenic fault were set as receiver faults and variant results followed. We provide a discussion on Coulomb stress transfer for the seismogenic fault, which is useful to identify potential future rupture zones.

Keywords Coulomb stress changes · Elastic model · Stress transfer · Earthquake risk · Nepal earthquake

1 Introduction

On April 25, 2015, the devastating M_W 7.8 Nepal earthquake struck the Himalayas of Nepal, collapsing buildings

X. Cheng (✉) · G. Meng
Institute of Earthquake Science, China Earthquake Administration, Fuxing Road 63, Haidian, Beijing, China
e-mail: chengxu126@126.com

and killing thousands of people in Nepal. Its aftershocks continued during the hours following this big earthquake (Fig. 1). Most aftershocks occurred to the southeast of the epicenter of the mainshock, of which five ones have the magnitudes of $M > 6$ up until May 15, 2015. Specifically, an M_W 7.3 aftershock occurred on May 12, 2015 approximately 130 km to the SEE of the mainshock and its focal mechanism is similar to that of the mainshock. Also, ∼ 110 km to the northeast of the mainshock there occurred a M_W 5.1 aftershock near Nyalam (China) about 11 hours later, while ∼ 250 km to the northeast of the mainshock an M_S 5.8 aftershock took place in Tingri County (China) just around 3 h later.

After the occurrence of this strong mainshock, many scientific workers conducted kinematic or dynamic modeling trying to understand the mechanism of its occurrence. For example, Shan et al. (2015) obtained the coseismic slip distribution model of this mainshock by joint inversion of InSAR and GPS data, and suggested that the MBT (Main Boundary Thrust) is the causative fault of the earthquake. Zhang et al. (2015) collected seismic data (P waves) and a few GPS data to carry out a joint inversion of rupture process, which showed the southeastward rupture propagation. Meanwhile, some workers probed the effect of the coseismic stress changes imparted by this strong earthquake. Wan et al. (2015) and Sheng et al. (2015) calculated the Coulomb stress changes (CSC) on Tibetan Plateau faults and Chinese mainland, and the result suggested that the Coulomb stress changes mainly have an effect on the Tibetan Plateau and Xinjiang (China). Using finite element method, Zhang et al. (2015) demonstrated that Coulomb failure stress changes in areas of Brahmaputra and the Lhasa block are positive and the magnitude is up to 10 kPa

Springer
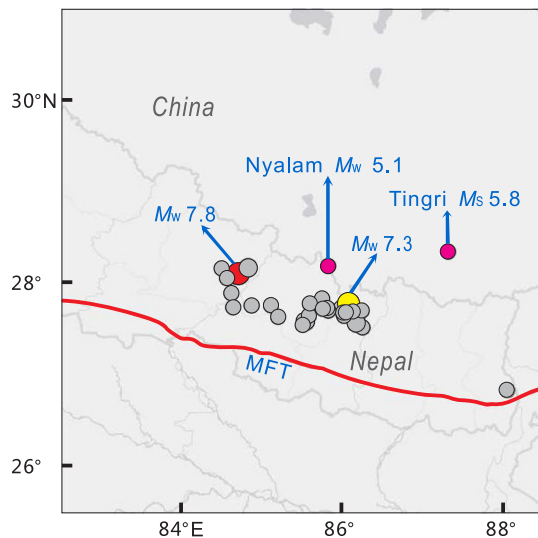
Fig. 1 The main event of the M_W 7.8 Nepal earthquake (*red filled circle*) and the aftershocks or other events from April 25 to May 15, 2015, for $M_\mathrm{W} > 5.0$. The *rose red filled circles* show Nyalam (*left* M_W 5.1) and Tingri (*right* M_S 5.8) earthquakes occurred almost the same day as the Nepal big shock. The *yellow filled circle* shows the M_W 7.3 aftershock occurred on May 12, 2015. The *red solid line* indicates the Himalayan Frontal Thrust. (Seismic data from NEIC)

for N–S trending normal faults, which implies possibilities of triggering strong earthquakes.

Coulomb stress changes induced by strong earthquakes are powerful to be used to examine relative stress state both in crust and on major faults as have been proved by lots of Coulomb stress studies worldwide. For example, In California, the 1992 M_W 7.3 Landers earthquake produced a lobe of positive Coulomb stress changes. This lobe is 40 km to the west of the mainshock, where the M_W 6.5 Big Bear earthquake struck 2.5 h afterwards (Stein 1999). In Turkey, the 1999 M_W 7.4 Izmit earthquake was followed by the M_W 7.1 Düzce earthquake that is a triggered event by the former about three months later (Parsons et al. 2000). In the 2008 Wenchuan event, some faults to the south of the Longmenshan fault exhibited increased transferred Coulomb stress (Parsons et al. 2008), especially the Ya'an thrust and Xianshuihe fault, which were shown to have distinctly greater changes in Coulomb stress than other faults. Later, Lushan (M_S 7.0) in April 2013 and Kangding (M_S 6.3) in November 2014 occurred near the Ya'an thrust and southern Xianshuihe faults, respectively. Previous research indicates that stress field changes caused by a large shock on the surrounding faults give rise to changes in seismicity rate in the vicinity (e.g., Wang et al. 2014; Stein 1999; Toda 1998).

Rearrangement of stresses in the crust commonly leads to subsequent damaging earthquakes (Stein et al. 1997; Stein 1999; Parsons et al. 2000; McCloskey et al. 2005). A

big earthquake can cause stresses on faults to decrease or increase, and it also alters stresses elsewhere (Parsons et al. 2000). Earthquakes are more prone to being observed in regions of increased stress, while they are less seen where off-fault stresses decrease (Stein 1999). Parsons et al. (2008) calculated the Coulomb stress changes after the 2008 Wenchuan earthquake showing a significant increase in stress on referring faults, which were basically coincident with the aftershocks or other earthquakes, such as the 2013 Lushan earthquake.

The Coulomb stress change model has been widely employed to explore the triggering and distribution of aftershocks (e.g., Toda et al. 2011; Hayes et al. 2014) and other mainshock triggering (Stein et al. 1997; Durand et al. 2013), and also to investigate regional hazards (Parsons et al. 2008; Maccaferri et al. 2013). In the similar way, it is necessary to calculate stress transfer in order to probe hazards and fault instability after the M_W 7.8 earthquake. Using the Coulomb stress-triggering hypothesis to calculate the stress field change can help us understand the failure potential of certain faults (Toda et al. 2011). Mapping such stress changes can help us comprehend trigger factors for earthquakes occurring nearby.

Previous studies (e.g., Wang et al. 2014) indicate that in some cases the Coulomb stress change is most sensitive to uncertainty in the dip angle of the receiver fault, while we cannot ignore the influences of uncertainties in the slip model for the source fault and the parameters of the receiver faults including strike, dip, and rake angles. Here, we use the Coulomb stress model to study changes in Coulomb stress after M_W 7.8 Nepal earthquake using the parameters of receiver faults with less uncertainties. On the basis of tectonic and fault structure background, we present calculations of the coseismic stress changes that resulted from the 25th April event using models of regional faults designed according to the structure of the Himalayas in South Tibet and Nepal. We show that some regional faults received significantly positive stresses. Based on the focal mechanism information from the U.S. Geological Survey (USGS) and the finite fault inversion results by Gavin Hayes (USGS/NEIC, http://earthquake.usgs.gov/earthquakes/eventpage/us20002926#scientific_finitefault), it seems that the mainshock of the event in Nepal ruptured along a shallow-dipping reverse fault to the north of the Main Frontal Thrust (MFT) between the Indian and Eurasian plates. The MFT seems to merge into the Main Himalaya Thrust (MHT) at a depth of ~ 5 km (Leloup et al. 2010; Ma and Gao 2011; Lavé and Avouac 2000), and the MHT is inferred to be the rupture fault along which many large earthquakes have occurred (Ader et al. 2012). Therefore, according to the inversion results from USGS finite faults, we set the source fault to be the MHT, where the M_W 7.8 Nepal event occurred, and the rupture fault dips

approximately 10° to the north near the surface to about 30 km depth under the Himalayan orogen. Also, we obtained the focal mechanism solution from the USGS to detailed slip directions. Then we set receiver faults on the basis of the regional tectonics and calculated stress transfers on these faults with a brief investigation of the stress-triggering factors of some events. Furthermore, we discuss the instability of the faults near the MFT in relation to earthquakes.

2 Methodology

We make our calculations using Coulomb 3.3 (Toda et al. 2005; Lin and Stein 2004) to estimate Coulomb stress along and across the rupturing fault in order to study the potential for future earthquakes on nearby faults or on a prescribed fault plane. The calculations are conducted in an elastic half-space with uniform isotropic elastic medium following the formulae of Okada (1992).

We calculate static stress changes caused by the displacement of a fault on which dislocations happen and an earthquake occurs. This fault is referred to as the 'source fault'. The displacements in the elastic half-space are used to calculate the 3D strain field; this is multiplied by elastic stiffness to derive stress changes. Shear and normal components of the stress change are calculated on a 3D grid of points or on specified 'receiver' fault planes. Receiver faults are planes with a specified strike, dip, and rake, on which the stresses imparted by the source fault are resolved.

For Coulomb failure criterion, we have

$$\Delta\sigma_f = \Delta\tau_s + \mu'\Delta\sigma_n. \tag{1}$$

Here $\Delta\tau_s$ is the change in shear stress (positive in the direction of fault slip), $\Delta\sigma_n$ is the change in normal stress (positive when the fault is unclamped), and μ' is the effective coefficient of friction on a fault (King et al. 1994). The stress tensors resulting from a source earthquake are projected onto a particular plane to obtain the shear and normal components of the stress change. $\Delta\sigma_f$ is the change in failure stress on a receiver fault caused by slip on the source fault. A positive $\Delta\sigma_f$ may promote fault closer to failure, and a negative value suppresses failure. The effective coefficient is assigned the value of 0.8 for continental thrust faults and 0.4 for strike-slip faults, based on Parsons et al. (1999) and others (Harris 1998; Cotton and Coutant 1997).

3 Tectonics and setting of receiver faults

The Himalaya orogenic belt consists of the MFT, the MBT, the Main Center Thrust (MCT), and the South Tibet Detachment System (STDS), all of which are aligned from south to north and are principally parallel (Ma and Gao 2011; Yin 2006). The three thrusts partition the Himalayan range, which is the archetype of a compressive thrust belt, into the Siwalik Himalaya (SH), the Lesser Himalaya (LH), and the High Himalaya Crystalline (HHC) in terms of petrography (Leloup et al. 2010). The MFT, which forms the boundary between Siwalik Himalaya and Quaternary deposits of the Ganges Plain (GP) (Liu et al. 2012), seems to merge with the MBT into the MHT at a depth of ∼5 km (Leloup et al. 2010; Ma and Gao 2011; Lavé and Avouac 2000). North of the MFT, the décollement of the Indian basement is thought to extend with flat geometry beneath the Lesser Himalaya and to form a steeper ramp at the front of the High Himalaya (Lavé and Avouac 2000). The MBT is a series of thrusts that separate the Lesser Himalaya sediments from the Tertiary Siwalik sedimentary belt (e.g., Leloup et al. 2010; Ni and Barazangi 1984). The MCT is a series of thrusts separating the High Himalaya from the Lesser Himalaya (ibid.). Both the MBT and the MCT dip northward are no longer very active (Takada and Matsu'ura 2007); only the youngest, southernmost thrust (MFT) appears to be active in central Nepal (Bollinger et al. 2014). Some studies have also suggested out-of-sequence thrusting, with possible thrust fault reactivation in the MCT zone (e.g., Hodges et al. 2004; Seeber and Gornitz 1983). The STDS shows normal faulting in a direction almost parallel to the direction of thrusting (Leloup et al. 2010; Burchfiel et al. 1992). There are also several normal rift systems featuring roughly N–S strike to the north of the STDS where the Tethyan sedimentary series (TSS) appears (Figs. 2, 3).

The Indian crust and lithospheric mantle underthrusts beneath the Himalaya and Tibet crust, and the Himalayan Orogen is pushed over a thrust fault zone, which is called a detachment fault. The shallow crust of the Himalayan front is carried northward due to the chain that couples both sides, although it has the potential to move southwards relative to the deeper part. Strain energy can increase due to strain accumulating as the northward motion continues. Earthquakes occur along the thrust faults when stress accumulation is highly enough. A previous study shows the inference that large earthquakes that are known to recur along the Himalayan front must be associated with ruptures of the MHT, which emerges at the surface along the front of the Himalayan foothills and is a major basal thrust fault (Ader et al. 2012). Besides this, to the north of the Himalayan Orogen, there are normal faults and graben structures, generally at N–S strike, which show west-east extension and are relevant to shallow normal style earthquakes (Ni and Barazangi 1984).
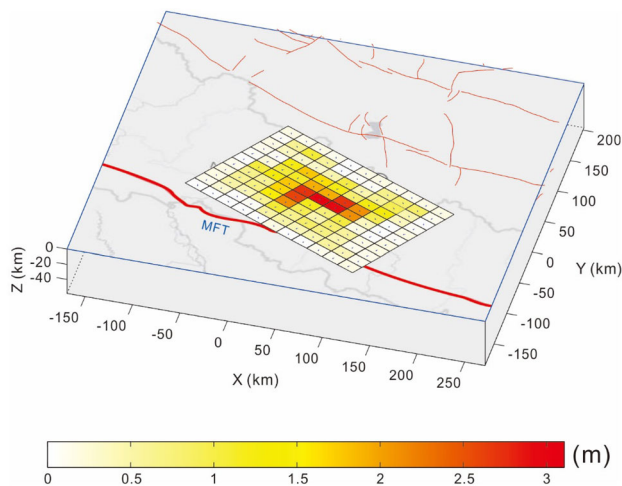
Fig. 2 Net slip on seismogenic fault according to finite fault solution inverted result from USGS
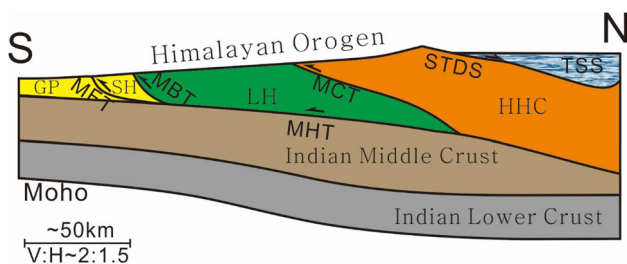

Fig. 3 Sketch of cross section through the central Himalayan orogenic belt (modified after Leloup et al. (2010), Ma and Gao (2011) and Rajendran K and Rajendran CP (2011)). *GP* Ganges Plain, *SH* Siwalik Himalaya, *LH* Lesser Himalaya, *HHC* high Himalaya crystalline, *TSS* Tethyan sedimentary series, *MFT* Main Frontal Thrust, *MBT* Main Boundary Thrust, *MCT* Main Central Thrust, *STDS* South Tibet Detachment System, *MHT* Main Himalayan Thrust

From the focal mechanism solutions, we can determine that the Himalaya region clearly has reverse fault rupture as far as the MCT. The MHT fault emerges at the surface along the front of the Himalayan foothills (e.g., Avouac 2003; Ader et al. 2012). The MFT dips about 30° (e.g., Rajendran et al. 2015) and the MBT about 60°–90° (e.g., Ni and Barazangi 1984). Both of them appear to merge with the MHT at depth—the plane of detachment, commonly referred to as the décollement (Fig. 2). The MCT dips 30°–45°, along which there are some geological indications of minor recent movement (e.g., Valdiya 1980). The MHT, dipping at about 10° to the north, exhibits a downdip end of the locked part of the fault about 100 km along dip from its surface trace (Ader et al. 2012). The STDS is a major normal fault system that runs parallel to the Himalayan range for more than 1500 km and dips gently 5°–15° to the north (Leloup et al. 2010). In the TSS zone, the Thakkhola graben (TG), the Kung Co rift (KC), and the Ama Drime Massif (AD) basically align from west

Table 1 Setting of receiver faults

Faults	Strikes	Dips	Rakes	Depth
DF	∼15°	70°	−80° to −100°	15 km
MF	∼215°	85°	−80° to −100°	15 km
NGF	∼190°	60°	−80° to −100°	15 km
KCF	∼164°	70°	−80° to −100°	15 km
KF	∼202°	50°	−80° to −100°	15 km
DgF	∼12°	50°	−80° to −100°	15 km

Dips and depth data here are set according to Baltz (2012), Yang et al. (2009), Lee et al. (2011), and Kali et al. (2010). Strikes and rakes here are set according to this model and normal fault

to east. Two primary normal faults, the Dangardzang fault (DF) and the Muktinath fault (MF), form the boundaries of the Thakkhola graben, dipping ∼70° to the east and 80°–90° to the west, respectively (Baltz 2012). A normal fault near the Gyirong basin (NGF) dips 50°–70° to the west (Yang et al. 2009). The Kung Co fault (KCF) refers to the Kung Co rift normal fault, dipping ∼70° roughly to the west (Lee et al., 2011). Another two normal faults, the Kharta fault (KF) and the Dinggye fault (DgF), bound the Ama Drime Massif (AD). The Kharta fault dips 45°–55° to the west, and the Dinggye fault dips ∼50° to the east (Kali et al. 2010). We set these 6 faults as the receiver faults (Table 1); they were grouped into four in terms of their locations (Fig. 4). We calculated the changes in Coulomb stress transferred on these active faults induced by the M_W 7.8 earthquake in Nepal on April 25, 2015.

The 25th April M_W 7.8 earthquake appears to have ruptured the main thrust fault, which may extend to the south surface; this is the MBT or MFT (Fig. 2). Tectonically, the MBT and MFT are shown to be more active than the MCT to the north due to their thrust and imbrication structure. The MHT reaches the surface at the MFT (Nakata 1989). The seismogenic Lamjung fault may lie along the MBT or MFT.

4 Results and discussion

4.1 Aftershocks

The M_W 7.8 event increased the stress beyond the east end of the rupture by 1–2 bars; this was where the greatest aftershock, of M_W 7.3, struck. It also increased the stress beyond the west end of the rupture by 0.5–5.0 bars, where a cluster of aftershocks occurred. Figure 5a shows the maximum value of Coulomb stress change between 0 and 20 km depth caused by the M_W 7.8 Nepal earthquake on optimally oriented thrust faults with N19°E regional compressive tectonic stress of 100 bars (10 MPa) and an effective coefficient of 0.8. The calculated stress increases
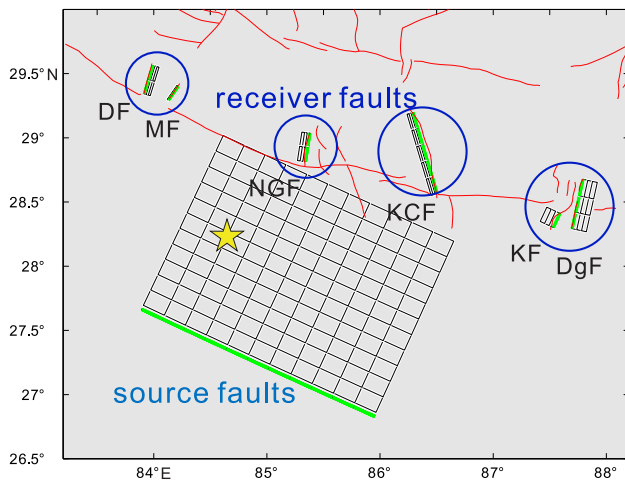
Fig. 4 Receiver faults are planes with a specified strike, dip, and rake, on which the stresses imparted by the source fault are resolved. Faults from the left to the right: *DF* Dangardzang fault, *MF* Muktinath fault, *NGF* normal fault near Gyirong basin, *KCF* Kung Co fault, *KF* Kharta fault, *DgF* Dinggye fault

are associated with heightened seismicity rates for aftershocks following the Nepal earthquake. Sites of decreased stress exhibit low seismicity rates. Figure 5b indicates that the aftershocks (gray dots; during the first 15 days after the mainshock, from the USGS) are associated with a zone of increased stress caused by the main rupture, such as the cluster southeast of the mainshock and the occurrence of the 12th May M_W 7.3 earthquake.

The aftershocks we used here are limited in 15 days after the mainshock. From the distribution of Coulomb stress changes for this Nepal earthquake, aftershocks region roughly corresponds to those positive high-value region of this elastic model.

4.2 Normal fault systems risk

There are many active faults to the north of the seismogenic fault in China (south Tibet), and some of them are located in villages. We attempted to set this type of faults in China to calculate Coulomb failure stress distribution. Given the elements of receiver faults we mentioned above, such as strike, dip, and rake, we calculated the Coulomb stress change for individual faults (Fig. 6). We set four groups of normal faults as the receiver faults (see the third part above) and three groups were shown to have increased Coulomb stress values up to 0.1 bar (0.01 MPa). The Coulomb stress in the easternmost group of faults, which belongs to the Dinggye normal fault system, increased the least (0.02–0.04 bar). This fault is near the 25th April M_S 5.8 Tingri earthquake, and Wan et al. (2015) indicated that the Tingri earthquake was triggered by the Nepal mainshock. Their calculation of Coulomb stress change on the
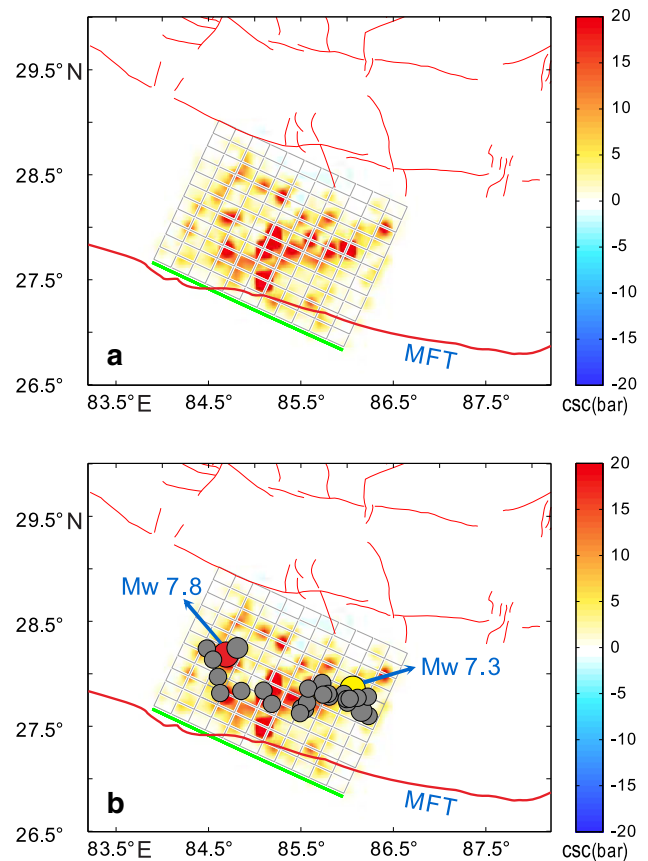

Fig. 5 Distribution of Coulomb stress changes on optimally oriented thrust faults and locations of the aftershocks. **a** The largest Coulomb stress changes between 0 and 20 km depth caused by the M_W 7.8 Nepal earthquake on optimally oriented thrust faults with the Main Frontal Thrust in *red solid line*. **b** Mainshock and aftershocks or other events between April 25, and May 15 , 2015

Tingri fault is 0.02–0.03 bar which is consistent with our findings. The westward fault, KCF, which locates near another M_W 5.1 Nyalam earthquake, has about 0.8–1 bar increased Coulomb stress in our model, and Wan et al. (2015) gave a result of 2–3 bar on their defined receiver fault, which is closer to the mainshock rupture zone than KCF.

Furthermore, there is not much difference here if the fault rake is changed (Fig. 7). Therefore, the normal faults to the north of the seismogenic faults mainly have increased Coulomb stress, and the western normal faults have a greater change in Coulomb stress than the easternmost faults. This indicates a greater risk from the western normal faults than from the easternmost faults. These normal faults are mostly located near villages in Gyirong County, Tingri County, and Dinggye County, for example. Thus, we should pay attention to studying these normal faults in the future.
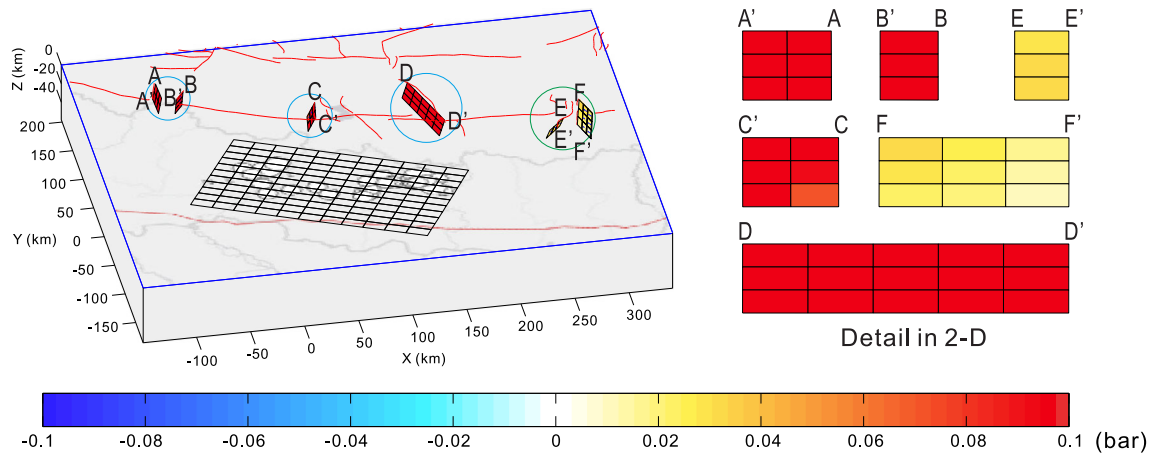
Fig. 6 Coulomb stress change on northern normal receiver faults: rakes, −90°; *blue circles* shows high increased value up to 0.1 bar (0.01 MPa) and *green circle* the lesser one
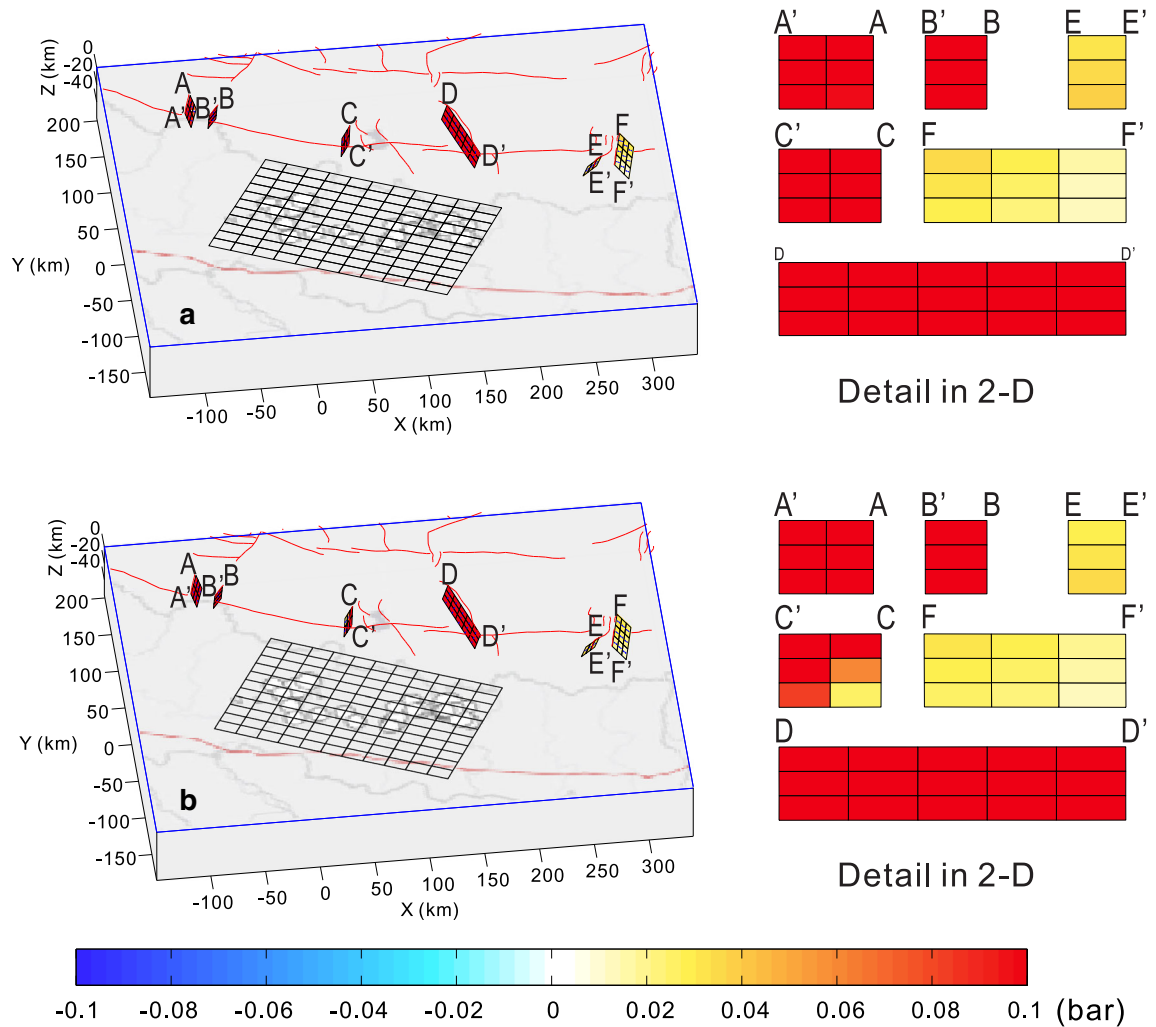

Fig. 7 Coulomb stress change on northern normal receiver faults with the rake angles of −80° (*top* subplot) and −100° (*bottom* subplot), respectively

4.3 MHT changes and predictions

In an interseismic period, the MHT is locked, and elastic deformation accumulates until it is released by large ($M_W > 8$) earthquakes (Lavé and Avouac 2000). These earthquakes break the MHT up to the near surface at the front of the Himalayan foothills and results in incremental activation of the MFT (ibid.). The pattern of coupling on the MHT is computed on a fault dipping 10° to the north and whose strike roughly follows the arcuate shape of the Himalayas (Ader et al. 2012). The MHT reaches the surface at the MFT (Nakata 1989) (Fig. 3), and the MHT is actually locked at the surface and roots about 100 km to the north of the MFT into a subhorizontal shear zone, which is probably thermally enhanced ductile flow (Cattin and Avouac 2000). Therefore, we set a receiver fault similar to the MHT and calculated the Coulomb stress change on that. We set roughly 20 km-depth MHT with a dip of 10° and a rake of 90°. Figure 8 shows the distribution of Coulomb stress change on the MHT; both ends of the MHT have increased Coulomb stress. It looks as though Coulomb stresses at the western part of the receiver fault increased more than those at the eastern part. The western part, at $10 \sim 20$ km, has clearly higher values up to 0.1 bar (0.01 MPa), which may indicate that the Coulomb stress increased more to the west than to the east of the seismogenic fault.

This result suggests that after the M_W 7.8 mainshock, there was a variation in stress response at each end of the seismogenic fault. The stress may have transferred to the west of the MHT more easily than to the east. A fairly large aftershock of M_W 7.3 occurred on May 12, 2015: that is, 17 days after the mainshock of M_W 7.8, which was located at the eastern part of the rupture fault. This event might have led to more sufficient rupture to the eastern part than to the west. There might be less stress transfer to the e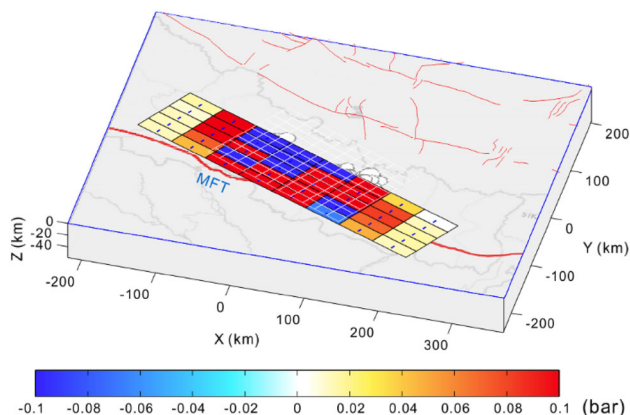ast of the MHT. To summarize, Coulomb stress may have transferred more to the west of the seismogenic fault than to the east after the Nepal earthquake and its aftershocks. This is useful for identifying potential future rupture zones and carrying out earthquake mitigation.

5 Conclusions

Coulomb stress change calculated from the elastic model can tell us the basic distribution of high-value stress changes corresponding to the distribution of aftershocks following the Nepal earthquake. Some normal faults (DF, MF, NGF, KCF, KF, DgF) to the north of the seismogenic fault mainly had increased Coulomb stress; Coulomb stresses at the western normal faults increased more than those at the easternmost faults, which indicates more risk from the western normal faults than from the easternmost faults. Hence, more attention should be paid to the west of the hypocenter of the mainshock.

Fig. 8 Coulomb stress changes on seismogenic fault

References

Ader T, Avouac JP, Jing LZ, Lyon-Caen H, Bollinger L, Galetzka J, Genrich J, Thomas M, Chanard K, Sapkota SN, Rajaure S, Shrestha P, Ding L, Flouzat M (2012) Convergence rate across the Nepal Himalaya and interseismic coupling on the Main Himalayan Thrust: implications for seismic hazard. J Geophys Res 117:B04403. doi:10.1029/2011JB009071

Avouac JP (2003) Mountain building, erosion and the seismic cycle in the Nepal Himalaya. Adv Geophys 46:1–79

Baltz T (2012) Structural evolution of Thakkhola Graben: implications for the architecture of the Central Himalaya, Nepal. A thesis presented to the Faculty of the Department of Earth and Atmospheric Sciences University of Houston

Bollinger L, Sapkota SN, Tapponnier P, Klinger Y, Rizza M, Van der Woerd J, Tiwari DR, Pandey R, Bitri A, Bes de Berc S (2014) Estimating the return times of great Himalayan earthquakes in eastern Nepal: evidence from the Patu and Bardibas strands of the Main Frontal Thrust. J Geophys Res Solid Earth 119:7123–7163. doi:10.1002/2014JB010970

Burchfiel BC, Zhilang C, Hodges KV, Yuping L, Royden LH, Changrong D, Jiene X (1992) The South Tibetan Detachment System, Himalayan Orogen: extension contemporaneous with and parallel to shortening in a collisional mountain belt. Geological Society of America 269:1–41. doi:10.1130/SPE269-p1

Cattin R, Avouac J (2000) Modeling mountain building and the seismic cycle in the Himalaya of Nepal. J Geophys Res 105:13389–13407. doi:10.1029/2000JB900032

Cotton F, Coutant O (1997) Dynamic stress variations due to shear faults in a plane layered medium. Geophys J Int 128:676–688. doi:10.1111/j.1365-246X.1997.tb05328.x

Durand V, Bouchon M, Karabulut H, Marsan D, Schmittbuhl J (2013) Link between Coulomb stress changes and seismic activation in the eastern Marmara Sea after the 1999, Izmit (Turkey), earthquake. J Geophys Res Solid Earth 118:681–688. doi:10.1002/jgrb.50077

Harris RA (1998) Introduction to special section: stress triggers, stress shadows, implications for seismic hazard. J Geophys Res 103(B10):24347–24358

Hayes GP, Furlong KP, Benz HM, Herman MW (2014) Triggered aseismic slip adjacent to the 6 February 2013 M_W 8.0 Santa Cruz Islands megathrust earthquake. Earth Planet Sci Lett 388:265–272. doi:10.1016/j.epsl.2013.11.010

Hodges KV, Wobus C, Ruhl K, Schildgen T, Whipple K (2004) Quaternary deformation, river steepening, and heavy precipitation at the front of the Higher Himalayan ranges. Earth Planet Sci Lett 220:379–389

Kali E, Leloup PH, Arnaud N, Mahéo G, Liu D, Boutonnet E, Van der Woerd J, Liu X, Jing LZ, Li H (2010) Exhumation history of the deepest central Himalayan rocks, Ama Drime range: key pressure-temperature-deformation-time constraints on orogenic models. Tectonics 29:2500–2522. doi:10.1029/2009TC002551

King GCP, Stein RS, Lin J (1994) Static stress changes and the triggering of earthquakes. Bull Seismol Soc Am 84:935–953

Lavé J, Avouac JP (2000) Active folding of fluvial terraces across the Siwaliks Hills, Himalayas of central Nepal. J Geophys Res 105:5735–5770

Lee J, Hager C, Wallis SR, Stockli DF, Whitehouse MJ, Aoya M, Wang Y (2011) Middle to late Miocene extremely rapid exhumation and thermal reequilibration in the Kung Co rift, southern Tibet. Tectonics 30:120–130. doi:10.1029/2010TC002745

Leloup PH, Mahéo G, Arnaud N, Kali E, Boutonnet E, Liu D, Liu X, Li H (2010) The South Tibet detachment shear zone in the Dinggye area: time constraints on extrusion models of the Himalayas. Earth Planet Sci Lett 292:1–16

Lin J, Stein RS (2004) Stress triggering in thrust and subduction earthquakes, and stress interaction between the southern San Andreas and nearby thrust and strike-slip faults. J Geophys Res 109:B02303. doi:10.1029/2003JB002607

Liu X, Hsu KJ, Ju Y, Li G, Liu X, Wei L, Zhou X, Zhang X (2012) New interpretation of tectonic model in south Tibet. J Asian Earth Sci 56:147–159. doi:10.1016/j.jseaes.2012.05.005

Ma XJ, Gao XL (2011) Transformation of tectonic movement and deformation partitioning across the Himalayan orogenic belt. Chinese J Geophys 54(6):1528–1535. doi:10.3969/j.issn.0001-5733.2011.06.012 (in Chinese with English abstract)

Maccaferri F, Rivalta E, Passarelli L, Jónsson S (2013) The stress shadow induced by the 1975–1984 Krafla rifting episode. J Geophys Res Solid Earth 118:1109–1121. doi:10.1002/jgrb.50134

McCloskey J, Nalbant SS, Steacy S (2005) Indonesian earthquake: earthquake risk from co-seismic stress. Nature 434:291

Nakata T (1989) Active faults of the Himalayas of India and Nepal. Spec. Pap. Geol. Soc. Am. 232:243–264

Ni J, Barazangi M (1984) Seismotectonics of the Himalayan Collision Zone: geometry of the Underthrusting Indian Plate Beneath the Himalaya. J Geophys Res 89:1147–1163

Okada Y (1992) Internal deformation due to shear and tensile faults in a half-space. Bull Seismol Soc Am 82:1018–1040

Parsons T, Stein RS, Simpson RW, Reasenberg PA (1999) Stress sensitivity of fault seismicity: a comparison between limited-offset oblique and major strike-slip faults. J Geophys Res 104:20183–20202

Parsons T, Toda S, Stein RS, Barka A, Dieterich JH (2000) Heightened odds of large earthquakes near Istanbul: an interaction-based probability calculation. Science 288(28):661–665

Parsons T, Ji C, Kirby E (2008) Stress changes from the 2008 Wenchuan earthquake and increased hazard in the Sichuan basin. Nature 454:509–510. doi:10.1038/nature07177

Rajendran K, Rajendran CP (2011) Revisiting the earthquake sources in the Himalaya: perspectives on past seismicity. Tectonophysics 504:75–88. doi:10.1016/j.tecto.2011.03.001

Rajendran CP, John B, Rajendran K (2015) Medieval pulse of great earthquakes in the central Himalaya: viewing past activities on the frontal thrust. J Geophys Res Solid Earth 120:1623–1641. doi:10.1002/2014JB011015

Seeber L, Gornitz V (1983) River profiles along the Himalayan arc as indicators of active tectonics. Tectonophysics 92(4):335–367

Shan XJ, Zhang GH, Wang CS, Liu YH (2015) Joint inversion for the spatial fault slip distribution of the 2015 Nepal M_W 7.9 earthquake based on InSAR and GPS observations. Chinese J Geophys 58(11):4266–4276 (in Chinese with English abstract)

Sheng SZ, Wan YG, Jiang CS, Bu YF (2015) Preliminary study on the static stress triggering effects on China mainland with the 2015 Nepal M_S 8.1 earthquake. Chinese J Geophys 58(5):1834–1842 (in Chinese with English abstract)

Stein RS (1999) The role of stress transfer in earthquake occurrence. Nature 402:605–609. doi:10.1038/45144

Stein RS, Barka AA, Dieterich JH (1997) Progressive failure on the North Anatolian fault since 1939 by earthquake stress triggering. Geophys J Int 128:594–604. doi:10.1111/j.1365-246X.1997.tb05321.x

Takada Y, Matsu'ura M (2007) Geometric evolution of a plate interface-branch fault system: its effects on the tectonic development of the Himalayas. J Asian Earth Sci 29:490–503

Toda S (1998) Stress transferred by the 1995 M_W 6.9 Kobe, Japan, shock: Effect on aftershocks and future earthquake probabilities. J Geophys Res 103:24543–24565

Toda S, Stein RS, Richards-Dinger K, Bozkurt S (2005) Forecasting the evolution of seismicity in southern California: animations built on earthquake stress transfer. J Geophys Res 110:361–368. doi:10.1029/2004JB003415

Toda S, Lin J, Stein RS (2011) Using the 2011 M_W 9.0 off the Pacific coast of Tohoku earthquake to test the Coulomb stress triggering hypothesis and to calculate faults brought closer to failure. Earth Planet Space 63(7):725–730. doi:10.5047/eps.2011.05.010

Valdiya KS (1980) The two intracrustal boundary thrusts of the Himalaya. Tectonophysics 66:323–348

Wan YG, Sheng SZ, Li X, Shen ZK (2015) Stress influence of the 2015 Nepal earthquake sequence on Chinese mainland. Chinese J Geophys 58(11):4277–4286 (in Chinese with English abstract)

Wang J, Xu C, Freymueller JT, Li Z, Shen W (2014) Sensitivity of Coulomb stress change to the parameters of the Coulomb failure model: a case study using the 2008 M_W 7.9 Wenchuan earthquake. J Geophys Res Solid Earth 119:3371–3392. doi:10.1002/2012JB009860

Yang XY, Zhang JJ, Qi GW, Wang DC, Guo L, Li PY, Liu J (2009) Structure and deformation around the Grirong basin, northern Himalaya, and onset of the south Tibetan detachment system. Sci

China (Series D) 52(8):1046–1058. doi:10.1007/s11430-009-0111-2

Yin A (2006) Cenozoic tectonic evolution of the Himalayan orogen as constrained by along strike variation of structural geometry, exhumation history, and foreland sedimentation. Earth Sci Frontiers 13(5):416–515 **(in Chinese with English abstract)**

Zhang B, Cheng HH, Shi YL (2015a) Calculation of the co-seismic effect of M_S 8.1 earthquake, April 25, 2015, Nepal. Chinese J Geophys 58(5):1794–1803 **(in Chinese with English abstract)**

Zhang Y, Xu LS, Chen YT (2015b) Rupture process of the 2015 Nepal M_W 7.9 earthquake: fast inversion and preliminary joint inversion. Chinese J Geophys 58(5):1804–1811 **(in Chinese with English abstract)**